PNAS NEXUS

PNAS Nexus, 2024, **4**, pgae568

https://doi.org/10.1093/pnasnexus/pgae568
Advance access publication 20 December 2024
Research Report

ZHX3 interacts with CEBPB to repress hepatic gluconeogenic gene expression and uric acid secretion

Wei Xuan Tan[a,b], Lillian Yuxian Lim[a], Nesha Afsha[a], Gloria Mei En Chan[a], Carmen Ching[a,c], Gokce Oguz[d], Suat Peng Neo[e], Safiah Mohamed Ali[f], Adaikalavan Ramasamy[d], Jayantha Gunaratne[e], Walter Hunziker[f], Chin Meng Khoo[b] and Adrian Kee Keong Teo[a,b,c,g,*]

[a]Stem Cells and Diabetes Laboratory, Institute of Molecular and Cell Biology (IMCB), Agency for Science, Technology and Research (A*STAR), Singapore 138673, Singapore
[b]Department of Medicine, Yong Loo Lin School of Medicine, National University of Singapore, Singapore 119228, Singapore
[c]Precision Medicine Translational Research Programme, Yong Loo Lin School of Medicine, National University of Singapore, Singapore 119228, Singapore
[d]Bioinformatics Consulting and Training Platform, Genome Institute of Singapore, A*STAR, Singapore 138672, Singapore
[e]Translational Biomedical Proteomics Laboratory, IMCB, A*STAR, Singapore 138673, Singapore
[f]Epithelial Polarity in Disease and Tissue Regeneration Laboratory; Department of Physiology, Yong Loo Lin School of Medicine, National University of Singapore, Singapore 117593, Singapore
[g]Department of Biochemistry, Yong Loo Lin School of Medicine, National University of Singapore, Singapore 117596, Singapore
*To whom correspondence should be addressed: Email: ateo@imcb.a-star.edu.sg
Edited By Christian Metallo

Abstract

ZHX3, which encodes for a transcriptional repressor, is associated with fasting blood glucose (FBG) levels and increased type 2 diabetes (T2D) risk but its role in cell types involved in glucose metabolism is not well understood. Here, we show that the deletion of *ZHX3* in the human pancreatic β-cell line EndoC-βH1 did not impair glucose-stimulated insulin secretion (GSIS) nor perturb its transcriptome. On the other hand, we found that ZHX3 represses the expression of gluconeogenic genes *PCK1* and *G6PC1* in the human hepatoma line HepG2. Transcriptomic analysis of *ZHX3*-deficient HepG2 cells revealed that the uric acid transporter gene *SLC17A1* was up-regulated, which consequentially led to increased uric acid secretion. High levels of uric acid could then impair GSIS in EndoC-βH1 cells. Subsequently, in-depth co-immunoprecipitation followed by mass spectrometry analysis of ZHX3 in HepG2 cells identified transcription factor CEBPB as its binding partner, required to repress the transcription of *PCK1*, *G6PC1*, and partially *SLC17A1* in HepG2 cells. Overall, our study uncovered the role of ZHX3 in regulating glucose metabolism in hepatocytes, thereby influencing FBG levels and their association with T2D risk.

Keywords: type 2 diabetes, ZHX3, hepatic glucose production, uric acid, SLC17A1

Significance Statement

ZHX3, which encodes for a transcriptional repressor, is associated with fasting blood glucose (FBG) levels and increased type 2 diabetes (T2D) risk but its role in cell types involved in glucose metabolism is not well understood. Here, we show that the loss of ZHX3 in human β-cell lines had no appreciable impact on β-cell transcriptome or insulin secretion function. We found ZHX3 to repress hepatic gluconeogenic gene expression, in concert with CEBPB. ZHX3 also represses hepatic uric acid secretion that can be detrimental to β-cell insulin secretion function. Overall, ZHX3 contributes to FBG and T2D risk by acting on the hepatocytes. Individuals with variants in *ZHX3* can potentially be treated by targeting the hepatic glucose production pathway.

Introduction

ZHX3 is a gene found to be associated with fasting blood glucose (FBG) levels (1–3) and increased type 2 diabetes (T2D) risk (2) in the European population. It encodes a transcriptional repressor that contains two C_2H_2 zinc finger domains and five homeodomains (4). Currently, there is limited understanding of the physiological function of ZHX3, except that it is mostly implicated in various cancers, where it can act as an oncogene (5–7) or a tumor suppressor (8–11). Therefore, its role in cell types involved in glucose metabolism, such as pancreatic β cells or the liver, is unclear.

Based on multitrait profiling, the *ZHX3* T2D risk locus was found to be associated with FBG levels but not fasting insulin levels or other insulin sensitivity traits such as BMI, suggesting that β-cell function may be implicated (2). In addition, *ZHX3* transcript expression was found to be lower in T2D islets when compared

Competing Interest: A.K.K.T. is a co-founder and shareholder of BetaLife Pte Ltd but is not employed by the same. All other authors declare that there are no relationships or activities that might bias, or be perceived to bias, their work.
Received: March 12, 2024. **Accepted:** December 11, 2024

with healthy islets (12). The finding that acute glucose stimulation in human islets represses *ZHX3* expression further indicates that it is a glucose-sensitive gene in islets (12). Last but not least, correlation analysis revealed that human islets with poorer glucose-stimulated insulin secretion (GSIS) stimulation index tended to have lower *ZHX3* levels (12). While the evidence points to a role for ZHX3 in β-cell biology and function, a direct mechanistic relationship has yet to be demonstrated.

Apart from the pancreatic islets, ZHX3 could also play a role in another metabolic tissue, the liver. Luciferase reporter assays suggested that ZHX3 could be repressing glycolytic genes *Pkm* and *Hk2* in rat hepatocytes (10). In a separate study, ZHX3 was found to bind onto the promoters of the gluconeogenic genes *Pck1* and *G6pc1* in the mouse liver upon refeeding, although it was not determined whether the binding results in gene activation or repression (13). The binding of ZHX3 to the *Pck1* promoter in mouse hepatocytes is dependent on insulin and the presence of the insulin response sequence on the *Pck1* promoter (13). These observations suggest that ZHX3 could mediate the repression of gluconeogenesis in hepatocytes. However, ZHX3 has yet to be directly perturbed in hepatocytes to test this hypothesis.

Here, we used human cellular models to examine the role of ZHX3 in regulating glucose metabolism in pancreatic β cells and hepatocytes, and its potential role in contributing to T2D development. While the loss of ZHX3 in human pancreatic β cells was found to exert limited direct effects on their GSIS function and transcriptome, the loss of ZHX3 in human hepatoma cells led to increased gluconeogenesis and uric acid secretion. Hyperuricemia could then impair GSIS in human β cells. Overall, our study demonstrated that the T2D risk association underlying *ZHX3* is likely mediated through the regulation of hepatic gluconeogenesis and uric acid secretion.

Results

Loss of ZHX3 does not affect GSIS and the transcriptome in human EndoC-βH1 cells

To first investigate whether ZHX3 plays a role in regulating insulin secretion in human pancreatic β cells, three different gRNAs (sg*ZHX3*-1, sg*ZHX3*-2, and sg*ZHX3*-3) were used to knockout (KO) *ZHX3*, with an empty CRISPR vector used as the control (termed as Empty; Fig. S1A). Sanger sequencing of gDNA (Fig. S1B) and western blot analyses (Fig. S1C) then showed that *ZHX3* was successfully KO in sg*ZHX3*-2 and sg*ZHX3*-3 EndoC-βH1 stable lines. Next, to determine whether the loss of ZHX3 affects the functionality of these β cells, we compared the insulin secretion capacity between the control and KO cells. GSIS assay showed that insulin secretion at low (2.8 mM) and high (16.7 mM) glucose, as well as the stimulation index, were not different between the Empty control and *ZHX3* KO EndoC-βH1 cells (Fig. S1D and E), indicating that the loss of ZHX3 did not affect the functionality of EndoC-βH1 cells.

To further understand the role of ZHX3 in human pancreatic β cells, we performed RNA-seq analysis on Empty and sg*ZHX3*-3 EndoC-βH1 cells (Table S1). Using a threshold of at least 2-fold change and false discovery rate (FDR) < 0.05, we only identified 41 and 39 genes that were significantly up- and down-regulated, respectively (Fig. S1F). RT-qPCR validation of some of the most differentially expressed genes (*BCAR4*, *CXCL8*, *SYNPO*, *GRM4*, and *TNR*) in terms of $\log_2$FC and FDR values (Fig. S1F) revealed that the expression of these genes was directionally consistent with the RNA-seq results but was not significantly different in sg*ZHX3*-3 EndoC-βH1 cells when compared with the Empty control (Fig. S1G–K). *CBLN4*, *SLC12A1*, and *HS3ST4* were not selected for the validation because they are very lowly expressed in EndoC-βH1 cells. Overall, our data indicated that the KO of *ZHX3* in EndoC-βH1 cells did not have any apparent effect on GSIS function and their transcriptome.

ZHX3 represses gluconeogenic genes PCK1 and G6PC1 in HepG2 cells

We next investigated the role of ZHX3 in hepatocytes by knocking out *ZHX3* in HepG2 cells using two different gRNAs (sg*ZHX3*-2 and sg*ZHX3*-9), with an empty CRISPR vector as the control (termed as Empty; Figs. 1A and B, S2A and B). ZHX3 has been reported to repress the promoter activity of rat *Pkm* and *Hk2* genes (10). To validate this in human liver cells, we performed RT-qPCR analysis of human *PKM* and *HK2* gene expression in the *ZHX3* KO HepG2 lines. However, the KO of *ZHX3* did not affect the expression levels of *PKM* and *HK2* genes in HepG2 cells (Fig. S2C and D). Although it was reported that ZHX3 binds to *Pck1* and *G6pc1* promoters in mouse hepatocytes upon refeeding (13), whether ZHX3 regulates their expression in human hepatocytes remains to be confirmed. We evaluated the expression of *PCK1* and *G6PC1*, and found that they were both up-regulated in *ZHX3* KO HepG2 cells when compared with the Empty control (Fig. 1C and D). Western blot analyses then confirmed that PCK1 and G6PC1 proteins were modestly up-regulated in *ZHX3* KO HepG2 cells (Figs. 1E and S2E and F). To further validate these findings, we also performed an siRNA knockdown of *ZHX3* in HepG2 cells (Fig. S2G), and independently confirmed the up-regulation of *PCK1* and *G6PC1* gene expression in *ZHX3*-depleted HepG2 cells (Fig. S2H and I).

To confirm that ZHX3 represses the expression of *PCK1* and *G6PC1* in HepG2 cells, we stably overexpressed ZHX3 with a FLAG and V5 tag at the N- and C-terminus, respectively, in *ZHX3* KO HepG2 cells for rescue experiments. It has been reported that ZHX3 protein expression is regulated by ubiquitination-mediated proteasomal degradation (5). Hence, to enhance the overexpression of ZHX3 protein, we treated the stable overexpression rescue lines with the proteasome inhibitor MG132, and observed that 10 μM of MG132 treatment can increase the protein levels of recombinant ZHX3 protein from 8 h onwards (Fig. S3A). Therefore, all ZHX3 rescue experiments were performed with 8 h of 10 μM MG132 treatment. Immunofluorescence analysis confirmed that FLAG-ZHX3-V5 can be successfully expressed and co-localized to the nucleus in HepG2 cells (Fig. S3B). Using these rescue lines, we evaluated the expression of *PCK1* and *G6PC1*, and found that the overexpression of ZHX3 could indeed repress their expression (Fig. S3C and D).

To further study the repression of *PCK1* and *G6PC1* transcriptional activity by ZHX3 in HepG2 cells, we performed luciferase reporter assays using luciferase constructs containing the human *PCK1* or *G6PC1* promoter sequence. It was reported that ZHX3 requires an intact insulin response sequence on the mouse *Pck1* promoter for binding (13). Similar to *Pck1* (14), the *G6pc1* promoter also harbors an insulin response sequence (15, 16). Therefore, we constructed luciferase reporter plasmids with the promoters of human *PCK1* and *G6PC1* containing the insulin response sequence. Luciferase assays showed that the overexpression of ZHX3 could repress the promoter activities of *PCK1* and *G6PC1* in HepG2 cells (Fig. 1F and G). The deletion (Δ) of the insulin response sequence did not abolish ZHX3 repression of *PCK1* promoter activity (Fig. 1H) but did abolish *G6PC1* promoter activity (Fig. 1I), suggesting that the ZHX3 repression of *G6PC1* transcription is dependent on the insulin response sequence. Overall, our data confirmed

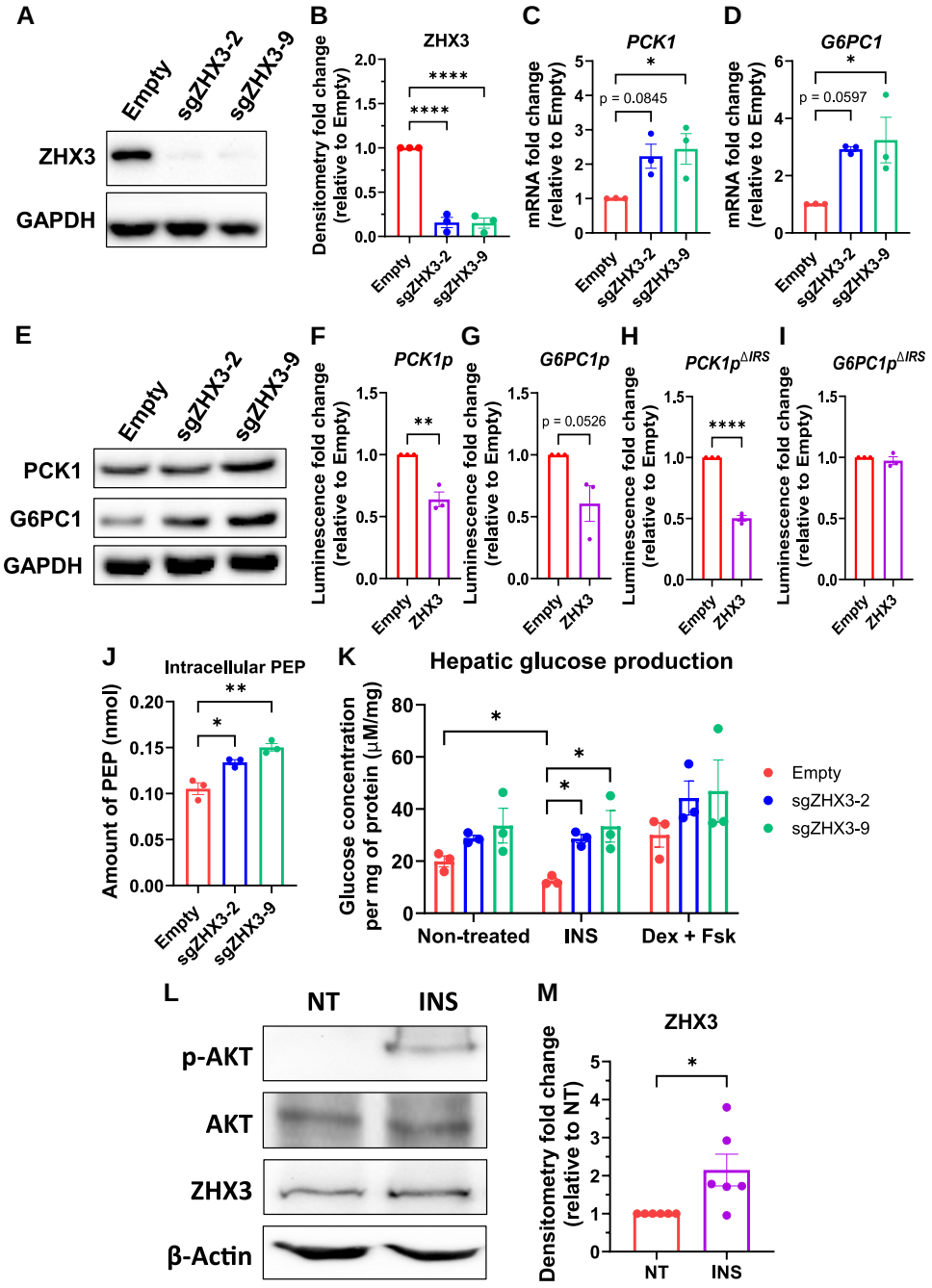

Fig. 1. ZHX3 represses the transcription of *PCK1* and *G6PC1* in HepG2 cells. A) Western blot analyses of ZHX3 in *ZHX3* KO HepG2 lines (one representative experiment) and B) the corresponding quantification graph ($n = 3$). ZHX3 protein levels were normalized to GAPDH protein levels. RT-qPCR analyses of C) *PCK1* and D) *G6PC1* in *ZHX3* KO HepG2 lines ($n = 3$). Data normalized to *ACTB* levels. E) Western blot analyses of PCK1 and G6PC1 in *ZHX3* KO HepG2 lines (one representative experiment). Luciferase analyses of F) *PCK1*, G) *G6PC1*, H) $PCK1^{\Delta IRS}$, or I) $G6PC1^{\Delta IRS}$ promoter in HepG2 cells overexpressed with Empty or FLAG-ZHX3-V5 vector ($n = 3$). Data normalized to Renilla luminescence values. IRS, insulin response sequence. J) Intracellular PEP measurement in *ZHX3* KO HepG2 lines ($n = 3$). K) HGP measurement in *ZHX3* KO HepG2 lines ($n = 3$). L) Western blot analyses of p-AKT, AKT, and ZHX3 in NT or INS-treated HepG2 cells (one representative experiment) and M) its corresponding quantification graph ($n = 6$). ZHX3 levels were normalized to GAPDH levels. Data presented as mean ± SEM. $^{*}P < 0.05$; $^{**}P < 0.01$; $^{****}P < 0.0001$. Statistical analyses were performed using unpaired t test or one-way ANOVA followed by Tukey's multiple comparison test. See also Figs. S2 and S3.

that ZHX3 can repress the transcription of gluconeogenic genes *PCK1* and *G6PC1* in HepG2 cells.

ZHX3 represses phosphoenolpyruvate and glucose production in HepG2 cells

The PCK1 enzyme controls the first rate-limiting step in gluconeogenesis, which is the conversion of oxaloacetate to phosphoenolpyruvate (PEP) (17, 18). The G6PC1 enzyme controls the last step of gluconeogenesis, which is the conversion of glucose-6-phosphate to glucose (19). Transcriptional regulation of these two enzymes is considered to be the main regulatory mechanism of hepatic glucose production (HGP) (20, 21). To investigate the impact of *PCK1* and *G6PC1* gene derepression upon the loss of ZHX3 in HepG2 cells, we measured the amount of PEP and HGP in *ZHX3* KO HepG2 cells. Consistent with our transcript

data, *ZHX3* KO HepG2 cells had higher PEP levels (Fig. 1J). We next performed a HGP assay on *ZHX3* KO HepG2 cells, under nontreated (NT), insulin (INS) treatment (simulating the fed state) or dexamethasone and forskolin (Dex + Fsk) treatment (simulating the starved state) conditions. Under NT and Dex + Fsk conditions, *ZHX3* KO HepG2 cells produced higher, albeit not statistically significant, levels of glucose when compared with the Empty control (Fig. 1K). This effect was more pronounced in the insulin-treated condition, where *ZHX3* KO HepG2 cells produced significantly higher levels of glucose than the Empty control (Fig. 1K). In addition, insulin repressed HGP in Empty control HepG2 cells but not *ZHX3* KO HepG2 cells, suggesting that ZHX3 could be mediating insulin's repression on HGP. Overall, our data suggest that ZHX3 represses the generation of PEP and HGP.

Insulin increases ZHX3 protein expression in HepG2 cells

The insulin response sequence is essential for insulin to repress mouse *G6pc1* transcription (15, 16). After demonstrating that ZHX3 requires the insulin response sequence to repress human *G6PC1* transcriptional activity (Fig. 1G and I) and insulin requires ZHX3 to repress HGP (Fig. 1K), we hypothesized that ZHX3 expression or activity could be regulated by insulin. To investigate this, we treated WT HepG2 cells with 100 nM of insulin for 1 h after an overnight serum starvation. Insulin stimulation increased the phosphorylation of AKT (Fig. 1L), indicating that insulin signaling was activated. Upon insulin stimulation, we observed an increase in ZHX3 protein expression (Fig. 1L and M), suggesting that insulin increases ZHX3 expression to repress *G6PC1* transcription and expression.

ZHX3 represses the urate transporter gene *SLC17A1* in HepG2 cells

To obtain an unbiased genome-wide understanding of the role of ZHX3 and the genes it regulates in hepatocytes, we performed RNA-seq analyses on Empty, sg*ZHX3*-2, and sg*ZHX3*-9 HepG2 cells. The transcriptome profile of *ZHX3* KO HepG2 cells was different from that of Empty control HepG2 cells (Fig. S4A). Using a threshold of at least 2-fold change and FDR < 0.1, we identified 184 and 55 genes that were commonly up- and down-regulated, respectively, in sg*ZHX3*-2 and sg*ZHX3*-9 HepG2 cells compared with Empty HepG2 cells (Table S2). Since ZHX3 is a known transcriptional repressor (4), we ran the overrepresentation analysis on the 184 up-regulated genes using g:Profiler (22) and interestingly, found urate metabolic process to be enriched (Fig. 2A). Over-representation analysis of the 55 down-regulated genes using g:Profiler did not yield any pathways in gene ontology (GO) biological processes (BPs). Volcano plot analysis of genes in the uric metabolic process showed *ABCG2*, *G6PC1*, *SLC17A1*, and *SLC17A3* to be significantly up-regulated in *ZHX3* KO HepG2 cells (Fig. 2B). *SLC17A1* was selected for characterization as a downstream target of ZHX3 based on its large fold change of up-regulation when compared with that of *ABCG2*, and the very low expression levels of *SLC17A3* in HepG2 cells.

We then performed RT-qPCR validation for *SLC17A1* and found that it was indeed up-regulated in both *ZHX3* KO (Fig. 2C) and si*ZHX3*-17 (Fig. S4B) HepG2 cells. Western blot analyses also confirmed SLC17A1 protein expression to be higher in *ZHX3* KO HepG2 cells when compared with Empty control HepG2 cells (Fig. 2D and E). We then evaluated the expression of *SLC17A1* in the ZHX3-rescued HepG2 cells and found that the overexpression of ZHX3 could indeed repress its expression (Fig. 2F). Consistently, luciferase reporter assays using *SLC17A1* promoter also showed that the overexpression of ZHX3 could repress its promoter activity (Fig. 2G). Overall, these results indicate that ZHX3 represses the transcription and expression of the uric acid transporter *SLC17A1* in HepG2 cells.

ZHX3 represses uric acid secretion from HepG2 cells that could be detrimental to insulin secretion from human β cells

SLC17A1 encodes a uric acid transporter (23) that exports uric acid in hepatocytes (24). The up-regulation of *SLC17A1* in *ZHX3* KO HepG2 cells prompted us to investigate whether these cells secreted more uric acid. First, we incubated WT HepG2 cells in serum-free (uric acid-free) media and measured the amount of uric acid in the media over time. Our data showed that the amount of uric acid in the media increased up to 24 h of incubation (Fig. 3A), indicating that HepG2 cells can secrete uric acid into the media. Next, uric acid secretion assays performed on sg*ZHX3*-2 and sg*ZHX3*-9 *ZHX3* KO HepG2 cells reflected an increase in uric acid secretion by 30–50% (Fig. 3B). Overexpression of ZHX3 was then able to repress the uric acid secretion in *ZHX3* KO HepG2 cells (Fig. 3C), confirming ZHX3 to be a negative regulator of uric acid secretion in HepG2 cells. Overall, our data reflected that the loss of ZHX3 can result in increased uric acid secretion from HepG2 cells.

Hyperuricemia has been shown to impair GSIS in rodent β cells (25–27). To determine whether this is also the case in human β cells, we treated EndoC-βH1 cells with doses that represent severe hyperuricemia, such as 10 or 30 mg/dL of uric acid (with NaOH as the vehicle control) and evaluated their viability and functionality. Neither 10 nor 30 mg/dL of uric acid treatment for 14 days affected the viability or proliferation of EndoC-βH1 cells, as assessed by the MTT assay (Fig. 3D). After 3 days of 10 or 30 mg/dL of uric acid treatment, we found that insulin secretion function was impaired in EndoC-βH1 cells, when compared with the NaOH vehicle control group (Fig. 3E). Overall, these results indicate that the loss of ZHX3 results in increased uric acid secretion from human hepatocytes. We postulate that the elevated uric acid levels could be detrimental to the insulin secretion function from human pancreatic β cells.

ZHX3 interacts with CEBPB to repress *PCK1*, *G6PC1*, and *SLC17A1* expression levels in HepG2 cells

To further investigate the mechanisms underlying ZHX3 repression of *PCK1*, *G6PC1*, and *SLC17A1* expression levels in HepG2 cells, we used co-immunoprecipitation (co-IP) assays, with the aim of identifying novel binding partners of ZHX3 (Fig. 4A). First, we showed that anti-FLAG antibody beads could pull down FLAG-ZHX3-V5 from lysates of MG132-treated HepG2 cells stably overexpressing FLAG-ZHX3-V5 (Fig. 4B). Second, ZHX3 has been reported to bind to the transcriptional activator NF-YA (4). To validate this, we performed western blot analysis of NF-YA in ZHX3 co-IP HepG2 lysates and found that ZHX3 does not bind to NF-YA in HepG2 cells (Fig. 4B). Having established that FLAG-ZHX3-V5 can be immunoprecipitated using anti-FLAG beads, we next performed double-labeling stable isotope labeling by amino acids in cell culture (SILAC) mass spectrometry (MS) analyses to identify novel binding partners of ZHX3 (Fig. 4A). Using a threshold of normalized SILAC ratio > 1.5 and ratio count > 1, we identified 45 and 39 proteins (in 2 separate experiments) that were significantly enriched in the ZHX3

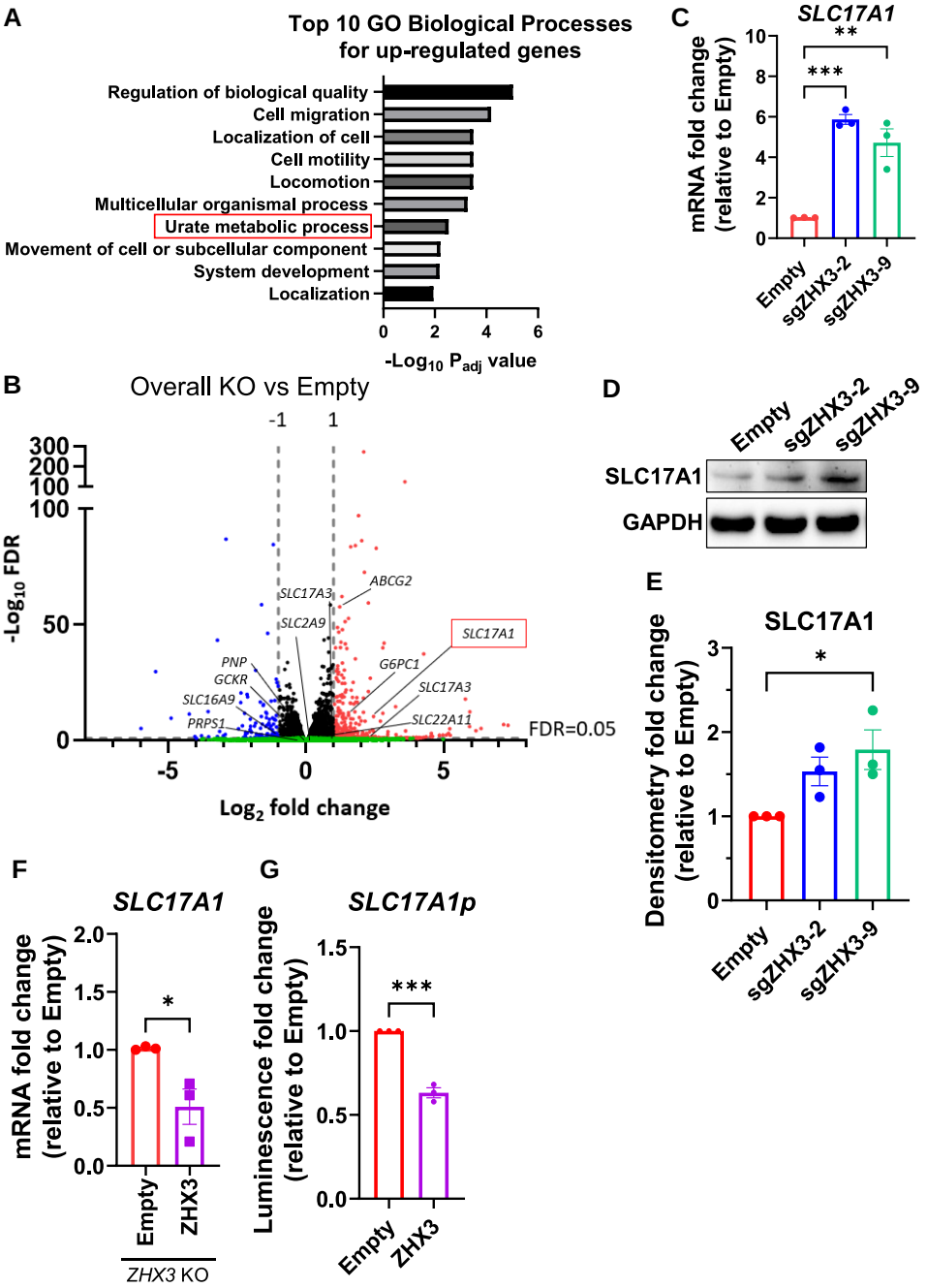

Fig. 2. ZHX3 represses the transcription of *SLC17A1* in HepG2 cells. A) Overrepresentation analysis of up-regulated genes in *ZHX3* KO HepG2 stable lines using g:Profiler and GO BPs. B) Volcano plot, with genes in the urate metabolic process pathway labeled. C) RT-qPCR analyses of *SLC17A1* in *ZHX3* KO HepG2 lines ($n = 3$). Data normalized to *ACTB* levels. D) Western blot analyses of SLC17A1 in *ZHX3* KO HepG2 lines (one representative experiment) and E) the corresponding quantification graph ($n = 3$). SLC17A1 protein levels were normalized to GAPDH protein levels. F) RT-qPCR analyses of *SLC17A1* in *ZHX3* KO HepG2 cells stably overexpressed with Empty or FLAG-ZHX3-V5 vector ($n = 3$). Data normalized to *ACTB* levels. G) Luciferase analyses of *SLC17A1* promoter in HepG2 cells overexpressed with Empty or FLAG-ZHX3-V5 vector ($n = 3$). Data normalized to Renilla luminescence values. Data presented as mean ± SEM. $^{*}P < 0.05$; $^{**}P < 0.01$; $^{***}P < 0.001$. Statistical analyses were performed using one-way ANOVA with Tukey's multiple comparison post hoc test. See also Figs. S2–S4.

pull-down samples when compared with the Empty pull-down controls (Tables S3 and S4). Among the proteins that were identified, eight were common across the two experiments, of which ZHX3 was, as expected, the top hit (Table 1). One notable hit was CEBPB, as CEBPB is a transcription factor known to activate the expression of gluconeogenic gene *PCK1* in hepatocytes (28–30). Therefore, we hypothesized that ZHX3 interacts with CEBPB to regulate the transcription of *PCK1* and *G6PC1* in HepG2 cells.

First, we confirmed the SILAC-MS data that ZHX3 binds to CEBPB protein via co-IP followed by western blot analyses (Fig. 4C). Next, we generated *CEBPB* and *ZHX3* double KO HepG2 stable cell lines (Fig. 4D and E). As expected, KO of *CEBPB* reduced *PCK1* and *G6PC1* expression levels (Fig. 4F and G). Notably, KO of *ZHX3* in *CEBPB*-deficient HepG2 cells did not result in a derepression of *PCK1* or *G6PC1* gene expression (Fig. 4F and G), suggesting that either (i) CEBPB is a critical activator without which there is nothing to repress by ZHX3 or (ii) ZHX3 requires CEBPB binding

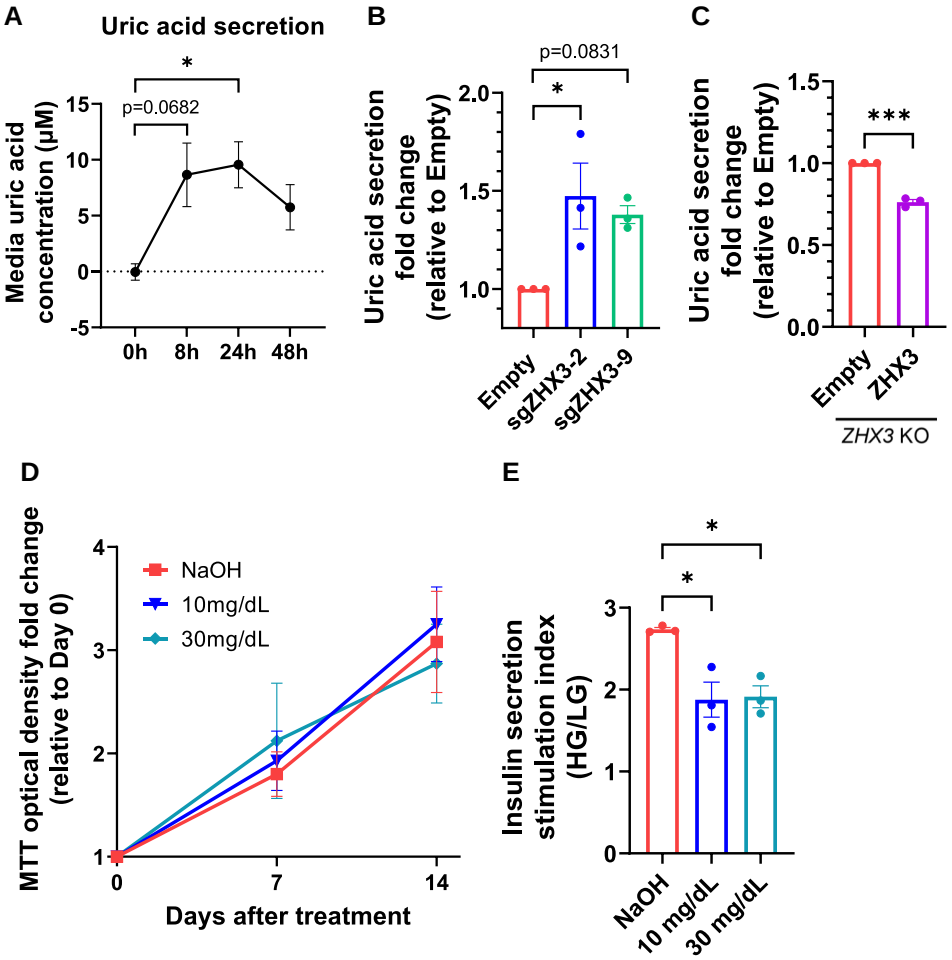

Fig. 3. KO of *ZHX3* leads to an increase in uric acid secretion in HepG2 cells that is detrimental to β-cell function. A) Time-course analyses of the amount of uric acid secreted into the media by WT HepG2 cells ($n = 3$). B) Uric acid secretion assay on *ZHX3* KO HepG2 stable lines ($n = 3$). Amount of uric acid secreted by each sample is normalized to its respective total protein content. C) Uric acid secretion assay on *ZHX3* KO HepG2 cells stably overexpressed with either the Empty or FLAG-ZHX3-V5 vector ($n = 3$). Amount of uric acid secreted by each sample is normalized to its respective total protein content. D) MTT assay on EndoC-βH1 cells treated with NaOH (vehicle control) or various concentrations of uric acid ($n = 3$). E) Insulin secretion stimulation index (high glucose [HG]/low glucose [LG]) of EndoC-βH1 cells treated with NaOH (vehicle control) or various concentrations of uric acid ($n = 3$). Data presented as mean ± SEM. $^*P < 0.05$. Statistical analyses were performed using one-way ANOVA with Tukey's multiple comparison post hoc test. See also Figs. S2 and S3.

to repress their transcription. While the KO of *CEBPB* also reduced *SLC17A1* expression levels (Fig. 4H), the KO of *ZHX3* in the *CEBPB*-deficient HepG2 cells could, however, derepress *SLC17A1* expression levels (Fig. 4H), albeit to a smaller extent compared with *ZHX3* KO HepG2 cells expressing functional CEBPB protein (Fig. 2C). This suggests that ZHX3 partially requires CEBPB to repress *SLC17A1* transcription.

Discussion

The *ZHX3* gene locus was found to be associated with T2D risk but its role in cell types involved in glucose metabolism, such as the pancreatic islets and liver, is not well understood. Here, we investigated the role of ZHX3 in glucose metabolism using various human cell models (Fig. S4C). Using EndoC-βH1 cells as a model for human β cells, we found that the loss of ZHX3 did not appear to affect cell functionality or transcriptomic profile, despite a previous study suggesting its implications with islets (12). Even though *ZHX3* transcript levels were found to be positively correlated with insulin secretion levels in human islets (12), correlation may not equate to causation. Moreover, islets contain other endocrine cell types, such as the α and δ cells, both of which have been shown to affect β cell insulin secretion (31–34). It is possible that while ZHX3 may not affect the β cells directly, ZHX3 can affect insulin secretion via other endocrine cell types. However, more work is needed to verify such dynamics.

Using HepG2 as a model for human hepatocytes, we found that ZHX3 expression is induced by insulin signaling and the loss of ZHX3 leads to an up-regulation of gluconeogenic genes *PCK1* and *G6PC1*. The up-regulation of these two genes led to increased PEP generation and HGP. The loss of ZHX3 also leads to an up-regulation of the uric acid transporter SLC17A1, which in turn increases uric acid secretion by HepG2 cells. Increased uric acid secretion by hepatocytes can lead to hyperuricemia (35), which we have shown to impair insulin secretion in human EndoC-βH1 cells. Overall, the loss of human ZHX3 could increase FBG levels and T2D risk by increasing hepatic gluconeogenesis, and hepatic uric acid secretion which impairs insulin secretion (Fig. S4C).

FBG levels are maintained primarily by HGP, and aberrant regulation of HGP can lead to fasting hyperglycemia and T2D (36). Here, we confirmed through various assays that ZHX3 represses the expression of *PCK1* and *G6PC1* in human hepatoma cells. In HepG2 cells, insulin activates ZHX3 expression and then ZHX3 represses *G6PC1*

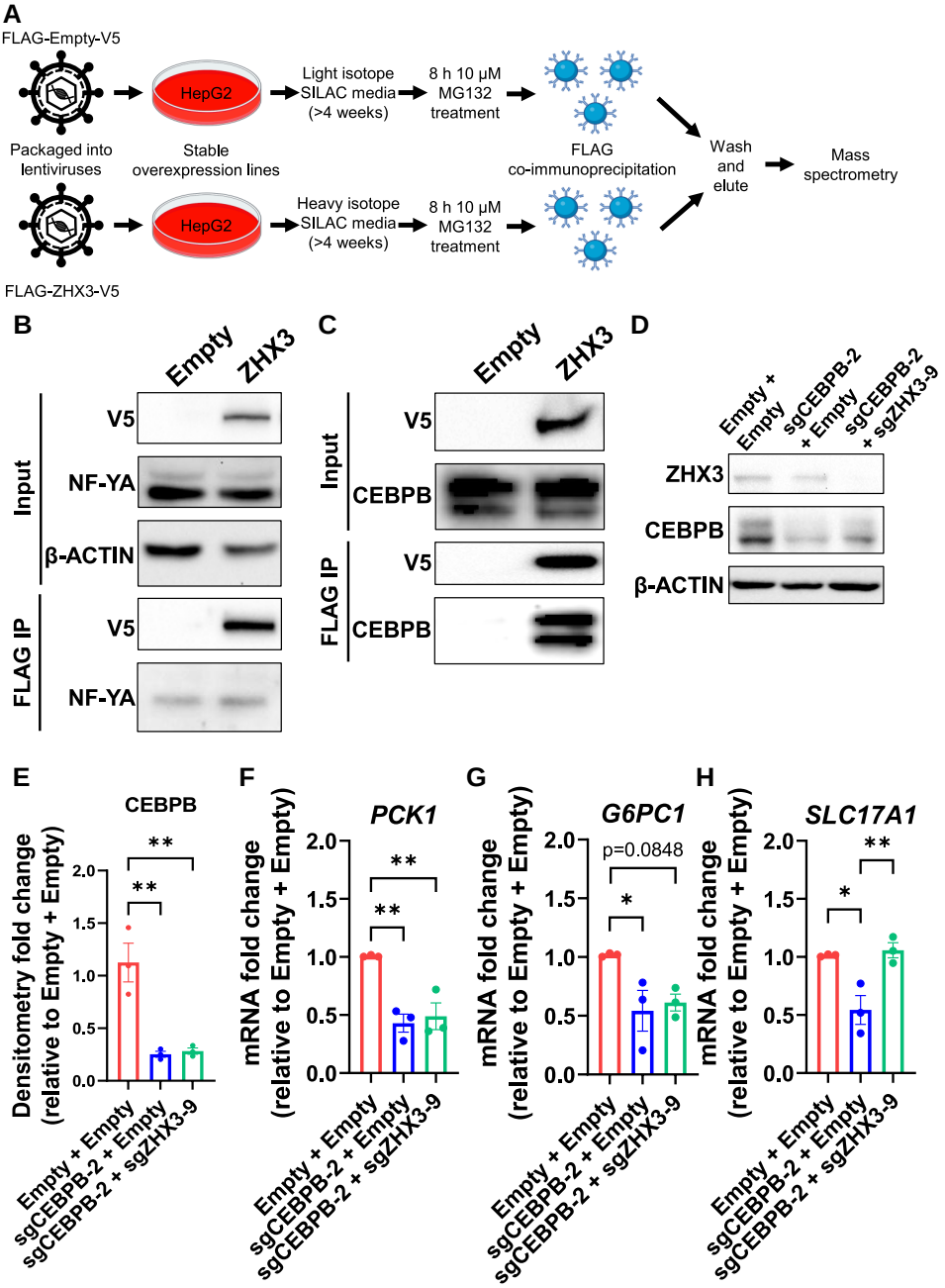

Fig. 4. ZHX3 interacts with CEBPB to repress the transcription of *PCK1*, *G6PC1*, and partially *SLC17A1* in HepG2 cells. A) Experimental design of identifying ZHX3-binding partners in HepG2 cells using SILAC-MS. Western blot analysis of B) NF-YA or C) CEBPB upon FLAG co-IP in HepG2 cells stably overexpressing Empty or FLAG-ZHX3-V5 vector. D) Western blot analyses of ZHX3 and CEBPB in *CEBPB* and *ZHX3* double KO HepG2 cells (one representative experiment) and E) the corresponding quantification graph ($n = 3$). RT-qPCR analyses of F) *PCK1*, G) *G6PC1*, and H) *SLC17A1* in *CEBPB* and *ZHX3* double KO HepG2 cells ($n = 3$). Data presented as mean ± SEM. $^{*}P < 0.05$; $^{**}P < 0.01$. Statistical analyses were performed using one-way ANOVA with Tukey's multiple comparison post hoc test.

gene expression in an insulin response sequence-dependent manner, indicating that ZHX3 could be a downstream mediator of insulin to repress gluconeogenesis. In line with this, *ZHX3* KO HepG2 cells produced more glucose under nontreated conditions, and this effect is even more pronounced under insulin-treated conditions. In addition, the loss of insulin-mediated repression on HGP in *ZHX3* KO HepG2 cells supports the notion that ZHX3 is a downstream mediator of insulin to repress HGP. This is consistent with a previous study reporting that ZHX3 binds to the promoter of *Pck1* and *G6pc1* only upon insulin stimulation in mouse hepatocytes (13). In the same study, it was shown that ZHX3 requires the insulin response sequence to bind to the *Pck1* promoter in mouse hepatocytes, while it was not shown for the *G6pc1* promoter (13). This discrepancy between our study and Wang et al. (13) could be due to species-specific differences.

We also found that ZHX3 interacts with CEBPB to repress the transcription of *PCK1* and *G6PC1* in HepG2 cells. CEBPB is responsible for maintaining the constitutive expression of these gluconeogenic genes in hepatocytes but its expression is also enhanced during fasting conditions (37). Importantly, *Cebpb*$^{-/-}$ mice die shortly after birth due to hypoglycemia, illustrating the role of CEBPB in activating HGP during fasting (28, 38). KO of *Cebpb* in mice did not affect glycogen storage in hepatocytes but affected their ability to mobilize

Table 1. Eight proteins commonly identified by two independent co-IP-MS experiments in HepG2 cells.

Protein	Experiment 1		Experiment 2	
	Normalized ratio (ZHX3/Empty)	Ratio count (ZHX3/Empty)	Normalized ratio (ZHX3/Empty)	Ratio count (ZHX3/Empty)
ZHX3	160.7	159	15.2	162
TPP1	5.3	13	4.3	7
ACADVL	4.2	2	2.0	7
CEBPB	2.3	3	1.5	3
MRPS25	2.2	2	8.5	2
XRCC5	1.9	32	1.8	58
XRCC6	1.9	22	1.9	58
TFB2M	1.6	2	1.8	3

it and activate hepatic *Pck1* expression (28, 38). Interestingly, we found that CEBPB regulates *SLC17A1* expression and that ZHX3 represses *SLC17A1* expression partly in concert with CEBPB in HepG2 cells. Overall, these findings unravel additional mechanisms in which ZHX3 interacts and cooperates with the transcription factor CEBPB to repress its target genes.

In the human liver cell model, we also found that the loss of ZHX3 in HepG2 cells led to an increase in hepatic uric acid secretion. Uric acid is mainly produced and secreted into the circulation by the liver (39). In humans, serum uric acid concentrations above 7 mg/dL are considered hyperuricemic, with 10 mg/dL found in severe hyperuricemic patients (40). Hyperuricemia is associated with a higher T2D risk (41, 42), insulin resistance (43) and β-cell dysfunction (44). Although it has been shown that hyperuricemia can impair insulin signaling in HepG2 cells (45, 46), hyperuricemia does not always result in insulin resistance in mice (25). Therefore, a causative role for hyperuricemia in insulin resistance may not be that straightforward and may involve other factors. On the other hand, hyperuricemia impairs both viability and GSIS function of rodent β cells via oxidative stress (25–27). High uric acid levels can induce the nuclear factor kappa B signaling pathway, leading to an increase in inducible nitric oxide (NO) synthase expression and NO levels, which induces apoptosis (25). Here, we showed that 10 and 30 mg/dL of uric acid impair GSIS function but not cell viability or proliferation of human EndoC-βH1 cells. Notably, it has been suggested that human islets are more resistant to oxidative stress than rodent islets (47–49), providing a possible explanation for the difference. Overall, our study showed that the hypersecretion of uric acid by hepatocytes due to the inactivation of hepatic ZHX3 can impair human β-cell function.

In summary, we uncovered the yet-unknown role(s) of ZHX3 in regulating FBG levels primarily in hepatocytes but not β cells. Upon insulin stimulation, ZHX3 exhibits an inhibitory role on hepatic gluconeogeneis by repressing the transcription of *PCK1* and *G6PC1*, and on hepatic uric acid secretion (which at high levels is detrimental to β-cell function) by repressing the transcription of *SLC17A1* (Fig. S4C). We posit that in T2D conditions, reduced circulatory insulin levels (reduced β-cell function) and diminished insulin effects on hepatocytes (insulin resistance) lead to lower hepatic ZHX3 expression, contributing to abnormally high HGP. Overall, this study provides evidence for *ZHX3* as the effector gene at the risk locus, to influence FBG levels and T2D risk.

Experimental model and subject details

Cell culture

HepG2 cells were cultured in Dulbecco's Modified Eagle Medium (DMEM) low glucose supplemented with 10% fetal bovine serum (FBS), 1% nonessential amino acids (NEAA) and 1× GlutaxMAX. EndoC-βH1 cells were cultured on tissue culture-treated dishes coated with 2 μg/mL of fibronectin and 1% of extracellular matrix in DMEM high glucose. For insulin treatment, HepG2 cells were serum-starved overnight before treatment with 100 ng of insulin for 1 h. The culture media for EndoC-βH1 cells consists of DMEM low glucose supplemented with 2% bovine serum albumin (BSA), 50 μM β-mercaptoethanol, 1% GlutaxMAX, 10 mM nicotinamide, 5.5 μg/mL human transferrin, and 6.7 ng/mL sodium selenite (50). All cells were tested negative for mycoplasma. All cells were incubated at 37 °C with 5% CO_2 and relative humidity of around 95%.

Method details

Generation of plasmids

To KO *ZHX3* in EndoC-βH1, three sgRNAs (sg*ZHX3*-1, sg*ZHX3*-2, and sg*ZHX3*-3; Resource Table) targeting exon 4 of human *ZHX3* were designed using the E-CRISP software (51). gRNAs were cloned into the lentiCRISPRv2 vector from Addgene (Plasmid 52961) with the EFS promoter replaced by a modified rat insulin promoter (RIP; lentiCRISPRv2-RIP), which was a gift from Dr Paul Gadue (52).

To KO *ZHX3* in HepG2 cells, we utilized the dimeric CRISPR RNA-guided FokI nuclease system (53). Briefly, two pairs of sgRNAs (sg*ZHX3*-2 and sg*ZHX3*-9; Resource Table) targeting exon 4 (first coding exon) of human *ZHX3* were designed using the ZiFit Targeter software and cloned into an all-in-one plasmid containing both pCAG-Csy4-T2A-dCas9-Fok1 and pU6-dual sgRNAs (53, 54).

To KO *CEBEB* in HepG2 cells, sg*CEBPB*-2 (Resource Table) was designed using CHOPCHOP (55) to target the first coding exon of human *CEBPB*. sg*CEBPB*-2 was cloned into the lentiCRISPRv2 vector from Addgene (Plasmid 52961).

To overexpress ZHX3, human *ZHX3* cDNA was amplified via PCR (using primers listed in Table S5) from EndoC-βH1 cDNA and cloned into the pCDH overexpression vector. The resulting vector, pCDH-FLAG-ZHX3-V5, expresses recombinant ZHX3 with a FLAG tag at the N-terminus and a V5 tag at the C-terminus. The vector also contains a GFP gene driven by an independent *EF1α* promoter.

For luciferase assays, the promoters of human *PCK1* (*PCK1p*; −1,847 to +38 relative to transcription start site [TSS]), *G6PC1* (*G6PC1p*; −1,947 to +53 relative to TSS) and *SLC17A1* (*SLC17A1p*; −1,190 to +120 relative to TSS) were amplified by PCR from HepG2 gDNA and cloned into the pGL4.10 luciferase vector. Primers used are listed in Table S5. These regions were selected to encompass potential ZHX3-binding motif (56) and the insulin response sequence (for *PCK1p* and *G6PC1p*) (14–16). To delete the insulin response sequence region in *PCK1p* (−395 to −381 relative to TSS) (13, 14) and *G6PC1p* (−185 to −157 relative to TSS) (15, 16), site-directed mutagenesis was performed using primers listed in Table S5.

Generation of lentiviruses

The pCDH and lentiCRISPRv2 plasmids were packaged into lentiviruses using a third-generation lentiviral system. 293FT cells were seeded onto 100 mm plates using a split ratio of 1:2.5 to achieve ∼90% confluency. The next day, lentiCRISPRv2 plasmids, packaging plasmids (pRC-CMV-Rev and pHDM-HIVgpm) and envelope plasmid (pHDM-VSV-G) were co-transfected into 293FT cells using the CalPhos transfection mix. Virus-containing media were collected at 48 and 72 h after transfection. After centrifugation and filtration through the 0.4 μm filter, lentiviruses were

pelleted using ultracentrifugation at 23,000 rpm for 90 min. The concentration of lentiviruses was quantified using the Lenti-X p24 Rapid Titer Kit.

Generation of stable lines in EndoC-βH1 cells

To generate *ZHX3* KO EndoC-βH1 stable lines, lentiCRISPRv2-RIP Empty (without any gRNAs), sg*ZHX3*-1, sg*ZHX3*-2, or sg*ZHX3*-3 vectors were packaged into lentiviruses and were used to transduce EndoC-βH1 cells at an MOI of 50 with 8 µg/mL polybrene. Forty-eight hours after transduction, cells were selected with 2 µg/mL puromycin for 5–7 days and maintained in 1 µg/mL puromycin as stable lines thereafter.

Generation of stable lines in HepG2 cells

For the generation of *ZHX3* KO HepG2 stable lines, HepG2 cells were transfected with either Empty (CRISPR vector without any gRNAs), sg*ZHX3*-2 or sg*ZHX3*-9 vectors. For transfection, 3 million HepG2 cells were seeded onto 6 cm tissue culture-treated plates and 8 µg of plasmids were transfected using Lipofectamine 2000 one day later. Forty-eight hours after transfection, cells were selected using 12 µg/mL of blasticidin for 6 days. Thereafter, cells were maintained in normal HepG2 growth media as stable lines.

For the generation of *CEBPB* and *ZHX3* double KO HepG2 stable lines, sg*CEBPB*-2 lentiCRISPRv2 vector was packaged into lentiviruses. For transduction, sg*ZHX3*-9 HepG2 cells were transduced with either empty or sg*CEBPB*-2 vector-containing lentiviruses at an MOI of 50 with 8 µg/mL polybrene. 48 h after transduction, cells were selected with 2 µg/mL puromycin for 5–7 days and maintained in 1 µg/mL puromycin as stable lines thereafter.

For the generation of HepG2 stable ZHX3 overexpression lines, pCDH-Empty (pCDH vector without any insert) or pCDH-FLAG-ZHX3-V5 vectors were packaged into lentiviruses. For transduction, either WT or sg*ZHX3*-2 HepG2 cells were transduced with the two overexpression vectors with an MOI of 30 with 8 µg/mL polybrene. Forty-eight hours after transduction, cells were selected with 2 µg/mL puromycin for 5–7 days and maintained in 1 µg/mL puromycin as stable lines thereafter.

Transfection

For luciferase assays, HepG2 cells were seeded at a density of 300,000 cells per well of a 24-well plate. In each well, HepG2 cells were co-transfected with pCDH overexpression (0.5 µg), pGL4.10 luciferase (0.4 µg) and pRL-TK renilla (10 ng) vectors. Transfection was performed with FuGENE HD Transfection Reagent at a FuGENE:plasmid ratio of 3:1 according to the manufacturer's protocol. Forty-eight hours after transfection, cells were harvested for luciferase assay.

GSIS and human insulin ELISA

EndoC-βH1 cells were seeded on 24-well plates at a density of 500,000 cells/well. Twenty-four hours after cell seeding, cells were first starved in Krebs–Ringer Bicarbonate (KRB) buffer (1 mM $CaCl_2$, 2.5 mM HEPES, 4.74 mM KCl, 1.2 mM K_2HPO_4, 1.2 mM $MgSO_4$, 125 mM NaCl, 5 mM $NaHCO_3$, and 0.1% fatty acid-free BSA) with 2.8 mM glucose for 1 h. Cells were then incubated in KRB buffer with 2.8 mM glucose for 1 h, followed by KRB buffer with 16.7 mM glucose for 1 h. The media in these two steps were collected for human insulin ELISA analysis. Before each step, cells were washed with KRB buffer. All incubations were done at 37 °C with 5% CO_2 and relative humidity of around 95%. The amount of insulin that was secreted into the media was quantified using the human insulin ELISA kit (Mercodia) as per the manufacturer's instructions. To calculate stimulation index, the amount of insulin secreted at high glucose levels was divided by that at low glucose levels.

Intracellular PEP assay

Two million HepG2 cells were collected during weekly passaging. After centrifugation, cell pellets were lysed in 100 µL of 3 M perchloric acid and subsequently neutralized with 3 M potassium bicarbonate to about pH 6.5 to 7.5. Thereafter, the amount of PEP was measured using the PEP assay kit (Abcam).

HGP assay

HepG2 stable lines were seeded on 6-well plates at a density of 1.5 million cells/well. Twenty-four hours after cell seeding, cells were serum-starved by incubating in serum-free HepG2 culture media overnight. Thereafter, cells were incubated in glucose-free and phenol red-free DMEM, supplemented with 4 mM L-glutamine, 20 mM sodium lactate, and 2 mM sodium pyruvate, with or without 100 nM insulin, or 1 µM dexamethasone, and 10 µM forskolin for 6 h. After the 6 h incubation, media were collected and centrifuged at 2,000 rpm for 5 min to remove any floating cells before the supernatant was collected for glucose assay. The concentration of glucose in the media was measured using the Amplex Red Glucose Assay Kit (Thermo Fisher Scientific). Cells were harvested for protein normalization.

Uric acid secretion assay

HepG2 stable lines were seeded on 12-well plates at a density of 600,000 cells/well. Twenty-four hours after cell seeding, cells were incubated in HepG2 culture media without FBS for 8, 24, and 48 h. For *ZHX3* KO HepG2 cells stably overexpressing Empty, FLAG-ZHX3-V5 vector, 10 µM MG132 was added into the medium. After 8 h, the media were collected and centrifuged to remove any floating cells before uric acid quantification using the Amplex Red Uric Acid/Uricase Assay Kit (Thermo Fisher Scientific). Cells were harvested for protein normalization.

RNA extraction and qPCR analysis

EndoC-βH1 cells were seeded onto 24-well plate at 500,000 cells/well in triplicates. HepG2 cells were seeded onto 24-well plate at 300,000 cells/well in triplicates. Cells were harvested 1 day after seeding. For HepG2 stable overexpression cells, cells were treated with 10 µM MG132 1 day after seeding for 8 h before being harvested. For mouse hepatocytes, hepatocytes from each mouse were seeded at 500,000 cells/well of a 12-well plate in DMEM high glucose + 10% FBS + 1% Pen/Strep. Three hours after cell seeding, media were replaced with DMEM low glucose + 10% FBS + 1% Pen/Strep and cells were incubated overnight before RNA extraction. RNA was extracted from samples via the NucleoSpin RNA Kit or the TRIzol reagent as per the manufacturer's protocol. RT was performed using the High-Capacity cDNA Reverse Transcription Kit as per the manufacturer's protocol. qPCR was set up using the iTaq Universal SYBR Green Supermix and 6.25 ng of cDNA in duplicates. Relative gene expression was analyzed using the $2^{-\Delta\Delta Ct}$ method. Primers used for qPCR are summarized in Table S5.

RNA-seq analysis

About 1 µg of RNA from EndoC-βH1 and HepG2 cells was sent to Novogene for total RNA sequencing. Triplicates for each genotype were sent for RNA-seq. A directional mRNA library prep was selected and at least 30 million reads were sequenced. Briefly, raw

reads were processed by using Trim Galore! v0.6.4 (57) to remove low-quality reads and trim adapters. Trimmed reads were then aligned to the human reference genome, hg38 using STAR v2.6.1d aligner (58) and FeatureCounts v1.6.4 (59) were used to assign reads. Finally, differential gene expression analysis was performed using the DESeq2 package (60), where genes showing at least 2-fold change and FDR < 0.05 or 0.1 when compared with the Empty control were considered as differentially expressed genes (DEGs). Over-representation analysis using g:Profiler was performed on the list of DEGs to identify significant GO BPs (22).

Protein isolation and western blot analysis

EndoC-βH1 cells were seeded onto a 6-well plate at 2.5 million cells/well. HepG2 cells were seeded onto a 6-well plate at 1.5 million cells/well. Cells were harvested one day after seeding by manual scraping in NP-40 lysis buffer (150 mM NaCl, 1% NP-40, 50 mM tris pH 8.0) with 1:100 protease inhibitors and phosphatase inhibitors before incubation on ice for 30 min with constant agitation. Protein concentrations were measured using the BCA Protein Assay Kit. For western blots, 20–50 µg of lysates were loaded into 8% sodium dodecyl sulfate–polyacrylamide gel electrophoresis (SDS–PAGE) gel. Proteins were blotted onto PVDF membrane via wet transfer. Membranes were blocked in 3–5% milk in tris-buffered saline + 0.01% Tween-20 (TBST) for an hour at room temperature, before overnight incubation with primary antibodies (Resource Table). Secondary antibody (Resource Table) incubations were done at room temperature for 1 h. Signals were developed using the SuperSignal West Dura Extended Duration Substrate and Bio-Rad ChemiDoc MP Imaging System.

Co-immunoprecipitation

HepG2 cells stably overexpressed with Empty or FLAG-ZHX3-V5 vectors were seeded in two 10 cm treated plates each at a density of 10 million cells/plate. Twenty-four hours after cell seeding, cells were treated with 10 µM of MG132 for 8 h before being harvested. Cells were manually scraped in cold phosphate-buffered saline (PBS). Cell pellets were lysed in NP-40 lysis buffer with 1:100 protease inhibitors and phosphatase inhibitors for 30 min on ice with constant agitation. Protein concentration was quantified by BCA assay and adjusted to 3 mg/mL. For each cell line, FLAG pulldown was performed by incubating 10 mg of protein with 20 µL of Anti-FLAG M2 Affinity Gel at 4 °C overnight. Subsequently, the anti-FLAG antibody-conjugated agarose beads were washed thrice with 1 mL of NP-40 lysis buffer before being heated at 99 °C for 5 min in 60 µL of SDS–PAGE loading buffer (41 µL of NP-40 lysis + protein and protease inhibitors, 15 µL of PAGE LDS Sample Buffer (4×) and 4 µL of 10× dithiothreitol). Twenty microliters of samples were loaded for western blot analysis.

For SILAC-MS, HepG2 cells stably overexpressed with Empty or FLAG-ZHX3-V5 vectors were cultured in "light" (Lys0Arg0) or "heavy" (Lys8Arg10), respectively, SILAC media supplemented with 10% dialyzed FBS, 1% GlutaxMAX, 1% NEAA, and 1% Pen/Strep for 4 weeks, where an incorporation test was carried out. After ensuring that heavy isotopes (K8R10) were successfully incorporated, cells were lysed for co-IP as described above. After overnight incubation with the anti-FLAG antibody-conjugated agarose beads, the "light" and "heavy" agarose beads were combined for washes, and immunoprecipitated proteins were eluted from the beads by heating at 99 °C for 5 min in 60 µL of SDS–PAGE loading buffer. The eluates were then separated by 1D 4–12% Bis–Tris protein PAGE gel, stained with Colloidal Blue, and thereafter protein bands were excised and digested using in-gel digestion procedures (61).

Mass spectrometry and data analysis

Tryptic peptides were subjected to Proxeon Liquid chromatography and Orbitrap Mass Spectrometry (Thermo Fisher Scientific) analysis, as described previously (62). Mass spectrometry raw data were processed by MaxQuant version 1.6.0.1 (63) using default settings and the Uniprot human database (2023 June release, 104,508 entries). Maximum FDRs were set to 0.01 for both peptides and proteins.

Luciferase assay

Luciferase assay was performed using the Dual-Luciferase Reporter 1000 Assay System assay (Promega) following the manufacturer's protocol. Briefly, cells were lysed in 100 µL of passive lysis buffer. After centrifugation, 20 µL of supernatant was transferred into a white flat-bottom 96-well plate. Fifty microliters of Luciferase Assay Reagent II were added and quantified using GloMAX 96 luminometer. Fifty microliters of Stop & Glo Reagent were then added and quantified again.

Immunofluorescence microscopy

Five hundred thousand HepG2 cells were seeded on coverslips, and cells were fixed in 4% paraformaldehyde the next day at room temperature for 15 min. Cells were then blocked in 5% donkey serum in PBS with 0.1% Triton X-100 at room temperature for 1 h, followed by primary antibody incubations at 4 °C overnight and secondary antibody incubations at room temperature for 1 h. Subsequently, cells were stained with DAPI (1:5000) at room temperature for 20 min. Cells were washed with PBS three times after each step. Lastly, cells on coverslips were mounted onto glass slides using DAKO fluorescence mounting medium. Images were taken using an Olympus Fluoview Inverted Confocal microscope.

Statistical analysis

Analysis was performed using Graphpad Prism version 9.0. When analyzing two groups, the unpaired t test was used. For comparison among three groups or more, either one-way or two-way ANOVA followed by a post hoc test (Tukey's single-tailed test) was used. Data are presented as mean ± SEM, and *n* is the number of independent experiments.

Acknowledgments

The authors thank Prof. Paul Gadue for sharing plasmids, Dr Elhadi Iich for supporting work on the RNA-seq data, and members of the Teo laboratory for the critical reading of this manuscript. Some of the images were created with BioRender.com. A.K.K.T. is the guarantor of this work and, as such, had full access to all the data in the study and takes responsibility for the integrity of the data and accuracy of the data analysis.

Supplementary Material

Supplementary material is available at *PNAS Nexus* online.

Funding

W.X.T. and C.C. are supported by the National University of Singapore (NUS) Research Scholarship. W.X.T. is also supported by NMRC OFYIRG24jan-0053 and the Paris-NUS PhD mobility

grant (ANR-18-IDEX-0001), where he was hosted by Prof. Raphael Scharfmann in the Institute Cochin, Paris for 3 months. L.Y.L. is supported by NMRC OFYIRG21jun-0035. A.K.K.T. is supported by IMCB, A*STAR, HLTRP/2022/NUS-IMCB-02, Paris-NUS grant 2021-2006-R/UP-NUS (ANR-18-IDEX-0001), OFIRG21jun-0097, CSASI21jun-0006, MTCIRG21-0071, SDDC/FY2021/EX/93-A147, FY 2022 Interstellar Initiative Beyond grant, H22G0a0005, I22D1AG053, HLCA23Feb-0031, SC36/19-000801-A044, and H24G1a0015.

Author Contributions

Conceptualization: W.X.T., C.M.K., and A.K.K.T. Methodology, writing—original draft: W.X.T. and A.K.K.T. Software: G.O. and A.R. Formal analysis: W.X.T., G.O., and A.R. Investigation: W.X.T., L.Y.L., N.A., G.M.E.C., C.C., G.O., S.M.A., and S.P.N. Resources: A.R., W.H., J.G., C.M.K., and A.K.K.T. Writing—review and editing: W.X.T., L.Y.L., N.A., G.M.E.C., C.C., G.O., S.P.N., S.M.A., A.R., J.G., W.H., C.M.K., and A.K.K.T. Supervision: C.M.K. and A.K.K.T. Project administration and funding acquisition: W.X.T. and A.K.K.T.

Data Availability

Further information and requests for resources and regents should be directed to and will be fulfilled by the lead contact, A.K.K.T. (ateo@imcb.a-star.edu.sg). All unique/stable reagents generated in this study are available from the lead contact without restriction. *ZHX3* KO EndoC-βH1 RNA-seq data are available on GEO (GSE236102). Secure token for reviewer access is gxazwkaelxenrer. *ZHX3* KO HepG2 RNA-seq data are available on GEO (GSE193872). Secure token for reviewer access is qtenkcuqnpydrub. Co-IP MS data are available in ProteomeXchange Consortium via the PRIDE [1] partner repository with the dataset identifier PXD046714, accessible via password M1PoPYQ5.

References

1 Mahajan A, *et al.* 2015. Identification and functional characterization of G6PC2 coding variants influencing glycemic traits define an effector transcript at the G6PC2-ABCB11 locus. *PLoS Genet*. 11:e1004876.
2 Mahajan A, *et al.* 2018. Refining the accuracy of validated target identification through coding variant fine-mapping in type 2 diabetes. *Nat Genet*. 50:559.
3 Scott RA, *et al.* 2012. Large-scale association analyses identify new loci influencing glycemic traits and provide insight into the underlying biological pathways. *Nat Genet*. 44:991.
4 Yamada K, *et al.* 2003. Analysis of zinc-fingers and homeoboxes (ZHX)-1-interacting proteins: molecular cloning and characterization of a member of the ZHX family, ZHX3. *Biochem J*. 373: 167–178.
5 Deng M, *et al.* 2021. ZHX3 promotes the progression of urothelial carcinoma of the bladder via repressing of RGS2 and is a novel substrate of TRIM21. *Cancer Sci*. 112:1758–1771.
6 Igata T, *et al.* 2022. Loss of the transcription repressor ZHX3 induces senescence-associated gene expression and mitochondrial-nucleolar activation. *PLoS One*. 17:e0262488.
7 You Y, *et al.* 2020. Prognostic value and therapeutic implications of ZHX family member expression in human gastric cancer. *Am J Transl Res*. 12:3376.
8 Kwon R-J, *et al.* 2017. Expression and prognostic significance of zinc fingers and homeoboxes family members in renal cell carcinoma. *PLoS One*. 12:e0171036.
9 Minamiya Y, *et al.* 2012. Suppression of Zinc Finger Homeobox 3 expression in tumor cells decreases the survival rate among non-small cell lung cancer patients. *Cancer Biomark*. 11:139–146.
10 Yamada K, *et al.* 2009. ZHX2 and ZHX3 repress cancer markers in normal hepatocytes. *Front Biosci (Landmark Ed)*. 14:3724–3732.
11 You Y, *et al.* 2019. Attenuated ZHX3 expression serves as a potential biomarker that predicts poor clinical outcomes in breast cancer patients. *Cancer Manag Res*. 11:1199–1210.
12 Ottosson-Laakso E, *et al.* 2017. Glucose-induced changes in gene expression in human pancreatic islets: causes or consequences of chronic hyperglycemia. *Diabetes*. 66:3013–3028.
13 Wang L, *et al.* 2019. Identification of insulin-responsive transcription factors that regulate glucose production by hepatocytes. *Diabetes*. 68:1156–1167.
14 O'Brien RM, Lucas PC, Forest CD, Magnuson MA, Granner DK. 1990. Identification of a sequence in the PEPCK gene that mediates a negative effect of insulin on transcription. *Science*. 249: 533–537.
15 Ayala JE, *et al.* 1999. Conservation of an insulin response unit between mouse and human glucose-6-phosphatase catalytic subunit gene promoters: transcription factor FKHR binds the insulin response sequence. *Diabetes*. 48:1885–1889.
16 Streeper RS, *et al.* 1997. A multicomponent insulin response sequence mediates a strong repression of mouse glucose-6-phosphatase gene transcription by insulin. *J Biol Chem*. 272: 11698–11701.
17 Hanson RW, Garber AJ. 1972. Phosphoenolpyruvate carboxykinase. I. Its ce: role in gluconeogenesis. *Am J Clin Nutr*. 25:1010–1021.
18 Yu S, Meng S, Xiang M, Ma H. 2021. Phosphoenolpyruvate carboxykinase in cell metabolism: roles and mechanisms beyond gluconeogenesis. *Mol Metab*. 53:101257.
19 Hutton JC, O'Brien RM. 2009. Glucose-6-phosphatase catalytic subunit gene family. *J Biol Chem*. 284:29241–29245.
20 Hatting M, Tavares CD, Sharabi K, Rines AK, Puigserver P. 2018. Insulin regulation of gluconeogenesis. *Ann N Y Acad Sci*. 1411: 21–35.
21 Zhang X, Yang S, Chen J, Su Z. 2019. Unraveling the regulation of hepatic gluconeogenesis. *Front Endocrinol (Lausanne)*. 9:802.
22 Raudvere U, *et al.* 2019. g:Profiler: a web server for functional enrichment analysis and conversions of gene lists (2019 update). *Nucleic Acids Res*. 47:W191–W198.
23 Iharada M, *et al.* 2010. Type 1 sodium-dependent phosphate transporter (SLC17A1 protein) is a Cl(-)-dependent urate exporter. *J Biol Chem*. 285:26107–26113.
24 Wada S, Matsunaga N, Tamai I. 2020. Mathematical modeling analysis of hepatic uric acid disposition using human sandwich-cultured hepatocytes. *Drug Metab Pharmacokinet*. 35:432–440.
25 Jia L, *et al.* 2013. Hyperuricemia causes pancreatic β-cell death and dysfunction through NF-κB signaling pathway. *PLoS One*. 8: e78284.
26 Xin Y, *et al.* 2018. Zurampic protects pancreatic β-cells from high uric acid induced-damage by inhibiting URAT1 and inactivating the ROS/AMPK/ERK pathways. *Cell Physiol Biochem*. 47:1074–1083.
27 Zhang Y, *et al.* 2013. Uric acid induces oxidative stress and growth inhibition by activating adenosine monophosphate-activated protein kinase and extracellular signal-regulated kinase signal pathways in pancreatic β cells. *Mol Cell Endocrinol*. 375:89–96.
28 Croniger CM, *et al.* 2001. Mice with a deletion in the gene for CCAAT/enhancer-binding protein β have an attenuated response

to cAMP and impaired carbohydrate metabolism. *J Biol Chem*. 276: 629–638.
29 Goldstein I, *et al*. 2017. Transcription factor assisted loading and enhancer dynamics dictate the hepatic fasting response. *Genome Res*. 27:427–439.
30 Park EA, *et al*. 1993. Relative roles of CCAAT/enhancer-binding protein beta and cAMP regulatory element-binding protein in controlling transcription of the gene for phosphoenolpyruvate carboxykinase (GTP). *J Biol Chem*. 268:613–619.
31 Hartig SM, Cox AR. 2020. Paracrine signaling in islet function and survival. *J Mol Med*. 98:451–467.
32 Hauge-Evans AC, *et al*. 2009. Somatostatin secreted by islet δ-cells fulfills multiple roles as a paracrine regulator of islet function. *Diabetes*. 58:403–411.
33 Holter MM, Saikia M, Cummings BP. 2022. Alpha-cell paracrine signaling in the regulation of beta-cell insulin secretion. *Front Endocrinol (Lausanne)*. 13:934775.
34 Moede T, Leibiger IB, Berggren P-O. 2020. Alpha cell regulation of beta cell function. *Diabetologia*. 63:2064–2075.
35 Terkeltaub RA. 2003. Gout. *N Engl J Med*. 349:1647–1655.
36 Lin HV, Accili D. 2011. Hormonal regulation of hepatic glucose production in health and disease. *Cell Metab*. 14:9–19.
37 Roesler WJ. 2001. The role of C/EBP in nutrient and hormonal regulation of gene expression. *Annu Rev Nutr*. 21:141–165.
38 Croniger C, *et al*. 1997. Role of the isoforms of CCAAT/enhancer-binding protein in the initiation of phosphoenolpyruvate carboxykinase (GTP) gene transcription at birth. *J Biol Chem*. 272: 26306–26312.
39 de Oliveira EP, Burini RC. 2012. High plasma uric acid concentration: causes and consequences. *Diabetol Metab Syndr*. 4:1–7.
40 Bardin T, Richette P. 2014. Definition of hyperuricemia and gouty conditions. *Curr Opin Rheumatol*. 26:186–191.
41 Jia Z, Zhang X, Kang S, Wu Y. 2013b. Serum uric acid levels and incidence of impaired fasting glucose and type 2 diabetes mellitus: a meta-analysis of cohort studies. *Diabetes Res Clin Pract*. 101: 88–96.
42 Lv Q, *et al*. 2013. High serum uric acid and increased risk of type 2 diabetes: a systemic review and meta-analysis of prospective cohort studies. *PLoS One*. 8:e56864.
43 Krishnan E, Pandya BJ, Chung L, Hariri A, Dabbous O. 2012. Hyperuricemia in young adults and risk of insulin resistance, prediabetes, and diabetes: a 15-year follow-up study. *Am J Epidemiol*. 176:108–116.
44 Ghasemi A. 2021. Uric acid-induced pancreatic β-cell dysfunction. *BMC Endocr Disord*. 21:1–5.
45 He F, *et al*. 2022. Autophagy protects against high uric acid-induced hepatic insulin resistance. *Mol Cell Endocrinol*. 547: 111599.
46 Wan X, *et al*. 2016. Uric acid regulates hepatic steatosis and insulin resistance through the NLRP3 inflammasome-dependent mechanism. *J Hepatol*. 64:925–932.
47 Eizirik DL. 1996. Beta-cell defence and repair mechanisms in human pancreatic islets. *Horm Metab Res*. 28:302–305.
48 Eizirik DL, *et al*. 1994. Major species differences between humans and rodents in the susceptibility to pancreatic beta-cell injury. *Proc Natl Acad Sci U S A*. 91:9253–9256.
49 Welsh N, *et al*. 1995. Differences in the expression of heat-shock proteins and antioxidant enzymes between human and rodent pancreatic islets: implications for the pathogenesis of insulin-dependent diabetes mellitus. *Mol Med*. 1:806–820.
50 Ravassard P, *et al*. 2011. A genetically engineered human pancreatic β cell line exhibiting glucose-inducible insulin secretion. *J Clin Invest*. 121:3589–3597.
51 Heigwer F, Kerr G, Boutros M. 2014. E-CRISP: fast CRISPR target site identification. *Nat Methods*. 11:122–123.
52 Cardenas-Diaz FL, *et al*. 2019. Modeling monogenic diabetes using human ESCs reveals developmental and metabolic deficiencies caused by mutations in HNF1A. *Cell Stem Cell*. 25: 273–289.e275.
53 Tsai SQ, *et al*. 2014. Dimeric CRISPR RNA-guided FokI nucleases for highly specific genome editing. *Nat Biotechnol*. 32: 569–576.
54 Havlicek S, *et al*. 2017. Re-engineered RNA-guided FokI-nucleases for improved genome editing in human cells. *Mol Ther*. 25: 342–355.
55 Labun K, *et al*. 2019. CHOPCHOP v3: expanding the CRISPR web toolbox beyond genome editing. *Nucleic Acids Res*. 47: W171–W174.
56 Liu G, Clement LC, Kanwar YS, Avila-Casado C, Chugh SS. 2006. ZHX proteins regulate podocyte gene expression during the development of nephrotic syndrome. *J Biol Chem*. 281: 39681–39692.
57 Krueger F. *Trim Galore!: a wrapper around Cutadapt and FastQC to consistently apply adapter and quality trimming to FastQ files, with extra functionality for RRBS data*. Babraham Institute, 2015.
58 Dobin A, *et al*. 2013. STAR: ultrafast universal RNA-seq aligner. *Bioinformatics*. 29:15–21.
59 Liao Y, Smyth GK, Shi W. 2014. featureCounts: an efficient general purpose program for assigning sequence reads to genomic features. *Bioinformatics*. 30:923–930.
60 Love MI, Huber W, Anders S. 2014. Moderated estimation of fold change and dispersion for RNA-seq data with DESeq2. *Genome Biol*. 15:1–21.
61 Shevchenko A, Tomas H, Havli J, Olsen JV, Mann M. 2006. In-gel digestion for mass spectrometric characterization of proteins and proteomes. *Nat Protoc*. 1:2856–2860.
62 Atherton P, *et al*. 2022. Tensin3 interaction with talin drives the formation of fibronectin-associated fibrillar adhesions. *J Cell Biol*. 221:e202107022.
63 Cox J, Mann M. 2008. MaxQuant enables high peptide identification rates, individualized ppb-range mass accuracies and proteome-wide protein quantification. *Nat Biotechnol*. 26: 1367–1372.